ACS OMEGA

Open Access

http://pubs.acs.org/journal/acsodf

Article

Investigation of Pipeline CO_2 Leakage and Diffusion on Offshore Platforms Based on Numerical Simulation

Yang Cao, Tao Liu, Guangchun Song,* Wei Zhou, Hui Han, Yuxing Li, Qihui Hu, and Ruidong Jing

Cite This: *ACS Omega* 2024, 9, 27537−27548

Read Online

ACCESS | Metrics & More | Article Recommendations

ABSTRACT: Pipeline transportation of CO_2 is the key link to realize carbon capture, utilization, and storage. CO_2 pipeline transportation may face the risk of leakage, which poses a great threat to the production process and personnel safety. It is of great significance to study the leakage and diffusion characteristics of CO_2 in pipeline transportation for the safety design and personnel protection of the offshore CO_2 storage platform. In order to study the leakage and diffusion characteristics of CO_2 in pipeline transportation on offshore platforms, a physical model of a target platform and several numerical models were built, and a series of pipeline CO_2 leakage and diffusion simulations were carried out using the method of numerical simulation. Based on the simulation results, the temperature distribution and CO_2 concentration distribution on the offshore platforms after leakage were measured and analyzed. The influence of leakage direction (horizontal and oblique 45° upward) was also studied. Dangerous areas on the platform and suggestions for staff evacuation were given according to the simulation results. The research results of this work can provide guidance for the safe operation of offshore CO_2 storage platforms.

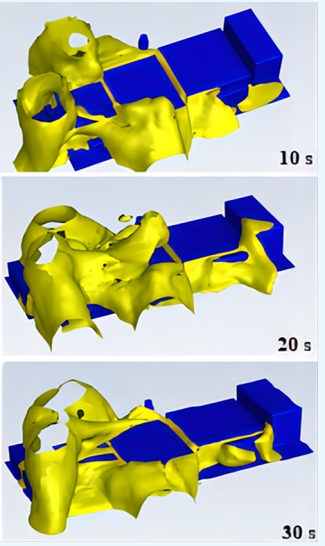

1. INTRODUCTION

Carbon dioxide (CO_2) is one of the leading greenhouse gases which could lead to global warming.[1] Carbon capture, utilization, and storage (CCUS) is an important way to reduce the emission of CO_2 and therefore mitigate the process of global warming.[2] As the key link of CCUS, the transportation of CO_2 through pipelines has received more and more attention and has developed significantly during recent years.[3−6] Usually, the captured CO_2 would be transported by the pipeline to storage places, among which the geological storages in the ocean is a good choice.[7,8] However, during the process of CO_2 pipeline transportation, the leakage and diffusion of CO_2 could frequently occur due to third party damages and corrosions,[9−12] which pose a great threat to the production process and personnel safety.[13,14] Therefore, it is of great importance to investigate the characteristics of the leakage and diffusion of pipeline CO_2.[15]

According to relevant researches, the process of pipeline CO_2 leakage mainly consists of near-field jet and far-field diffusion.[16,17] Until now, a lot of scholars and research institutes have conducted their work to study the characteristics of pipeline CO_2 leakage and diffusion. Wang et al.[18] investigated the dispersion behavior of CO_2 during the leakage of a high pressure pipeline. In their work, a laboratory scale experimental apparatus with a total length of 14.85 m and an inner diameter of 15 mm was used and the vertical leakage of CO_2 with different phase states through an orifice of 1 mm were conducted. Teng et al.[19] studied the leakage of supercritical CO_2 using a high pressure vessel. The effects of the size (1−5 mm) and pattern (circular and rectangular) of the leakage orifices were mainly investigated. Using the same experimental setup, Teng et al.[20] also studied the evolution and size distribution of solid CO_2 particles during the leakage process of supercritical CO_2. This literature focuses on the observation of the CO_2 jet flow field close to the leakage point, which helps us to investigate whether the near-field jet looks correct in the simulations Although the generation of dry ice was not considered in this simulation, it is the goal of future work. Guo et al.[21] investigated the jet flow and dispersion of supercritical CO_2 leakage through a large-scale pipeline with a length of 258 m and an inner diameter of 233 mm. By conducting experiments in the same setup, Guo et al.[22]

Received: March 28, 2024
Revised: May 15, 2024
Accepted: May 23, 2024
Published: June 11, 2024

also studied the fluid pressures, fluid temperatures, and wall temperatures along the along the pipeline during the leakage. The COSHER JIP (CO2 Safety, Health, Environment and Risk—Joint Industry Project)[23] carried out a series of large-scale pipeline leakage experiments using a 226.6 m long and 219.1 mm diameter flow loop. Witlox et al.[24,25] also performed several large-scale experiments using a vessel with leakage orifice (25−150 mm) conducted by the CO_2PIPETRANSJIP (Safe, Reliable and Cost-effective Transmission of Dense CO_2 in Pipelines, Joint Industry Project). The temperature and concentration of the dispersing CO_2 cloud were measured and analyzed during their work. Ahmad et al.[26] analyzed the characteristics of CO_2 leakage using a vessel with a 6.35 mm orifice. The effects of pressure (4−10.5 MPa) on CO_2 leakage were mainly studied. Xie et al.[27] investigated the upward leakage of CO_2 using a flow loop with a length of 23 m and an inner diameter of 30 mm. The above-mentioned literature helps to study the concentration and temperature fields of CO_2 in the atmosphere as it spreads after a leak and helps to identify the distance at which the safety of workers is threatened and the classification of hazardous areas when pipeline CO_2 leakage occurs during the actual production process in the simulation work.

It should be noted that as the key hub in an offshore CCUS project, the offshore platforms also face the danger of CO_2 pipeline leakage. However, at present, almost no systematic study has been carried out to investigate the characteristics of pipeline CO_2 leakage and diffusion on offshore platforms, which is worthy of further study. Considering that the actual size of the offshore platform can be very large, it is hard to construct an experimental setup which has the same size as the real platform. Under these circumstances, a numerical simulation can be a good choice.

Therefore, in this work, a physical model of the target offshore platform is constructed and is then used in a series of numerical simulations. The target offshore platform is produced by the China National Offshore Oil Corporation (CNOOC). Using a numerical simulation method, a series of pipeline supercritical CO_2 leakage and diffusion simulations are conducted in order to study the effects of leakage pressure, leakage time, ambient wind speed, leakage orifice size, and leakage direction on the leakage and diffusion of CO_2 on the offshore platform. The results of this study can provide guidance for the safe operation of offshore CO_2 storage platforms.

2. NUMERICAL SIMULATION

2.1. Physical Modeling. In this work, 3D modeling of the upper and middle layers of the target offshore platform is carried out by SpaceClaim software. The actual length of the offshore platform is 98.7 m, the width is 38 m, and the height is 14 m. In order to reduce the number of grids and improve the calculation accuracy, a cuboid external flow field structure with a length of 100 m, a width of 40 m, and a height of 16 m is established. The offshore platform model with external flow field is shown in Figure 1.

The mesh of the physical model is divided by Fluent Meshing software, and the offshore platform mesh is divided by a polyhedral core. The number of generated grids on the upper layer of the offshore platform is 570000, and the orthogonal mass is greater than 0.1, which is shown in Figure 2 as an example. The middle layer of the offshore platform is more complex due to the platform structure, and the number of grids is 1.1 million. The mesh for this simulation was not verified for irrelevance, as it meets the industrial requirements, and the simulated data obtained was compared with the experimental data to verify the accuracy.

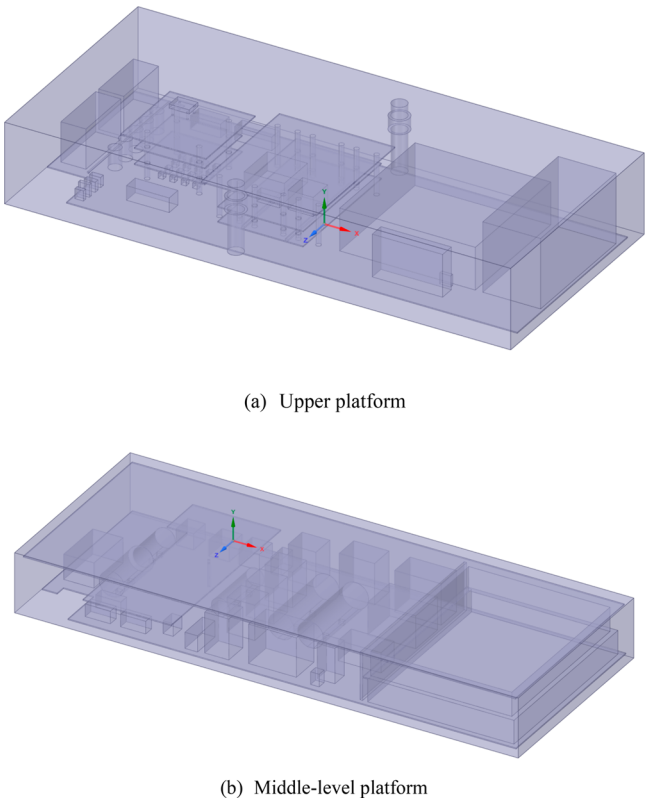

(a) Upper platform

(b) Middle-level platform

Figure 1. Computational domain of the offshore platform model.

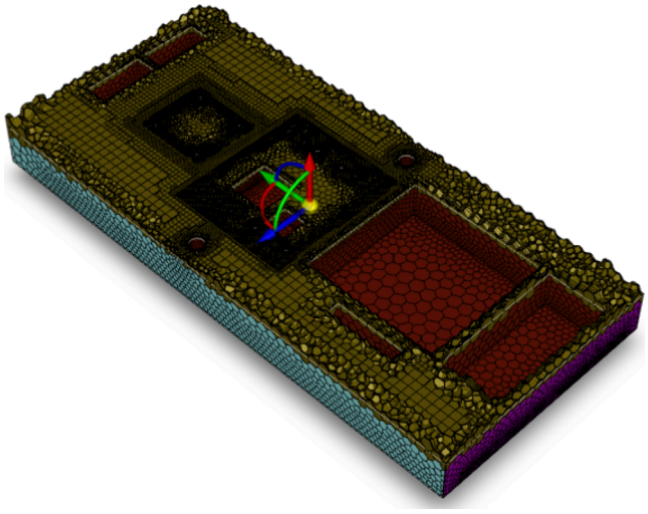

Figure 2. Upper model grid division of the offshore platform.

2.2. Numerical Models. After the leakage of supercritical CO_2, the three laws of momentum, energy, and mass conservation are followed in the external flow field, and the continuity equation, momentum equation, and energy equation need to be solved.

continuity equation:

$$\frac{\partial}{\partial t}(\rho_m) + \nabla\cdot(\rho_m \vec{v}_m) = 0 \quad (1)$$

https://doi.org/10.1021/acsomega.4c03002
ACS Omega 2024, 9, 27537−27548

momentum equation:

$$\frac{\partial}{\partial t}(\rho_m \overrightarrow{v_m}) + \nabla\cdot(\rho_m \overrightarrow{v_m}\overrightarrow{v_m}) = -\nabla p + \nabla\cdot[\mu_m(\nabla \overrightarrow{v_m} + \nabla v_m^T)] + \rho_m \vec{g} + \vec{F} - \nabla\cdot(\alpha_k \rho_k \overrightarrow{v_{dr,k}}\overrightarrow{v_{dr,k}}) \quad (2)$$

energy equation:

$$\frac{\partial E}{\partial t} + \frac{\partial}{\partial x_i}[(E + \vec{p})u_i - u_i\overline{u_i' u_j'}] = -\frac{\partial}{\partial x_i}\left(\lambda \frac{\partial T}{\partial x_i}\right) + S_E \quad (3)$$

CO_2 mass fraction equation:

$$\frac{\partial}{\partial t}(\alpha\rho) + \frac{\partial}{\partial x}(\alpha\rho \overrightarrow{u_i}) = \frac{\partial}{\partial x}\left(\mu_t \frac{\partial \alpha}{\partial x}\right) + S_\alpha \quad (4)$$

turbulence equations:

$$\frac{\partial}{\partial t}(\rho k) + \frac{\partial}{\partial x_i}(\rho k u_i) = \frac{\partial}{\partial x_j}\left(\Gamma_k \frac{\partial k}{\partial x_j}\right) + G_k - Y_k + S_k + G_b$$

$$\frac{\partial}{\partial t}(\rho\omega) + \frac{\partial}{\partial x_i}(\rho\omega u_i) = \frac{\partial}{\partial x_j}\left(\Gamma_\omega \frac{\partial \omega}{\partial x_j}\right) + G_\omega - Y_\omega + S_\omega + G_{\omega b} \quad (5)$$

In the formula, E is the total energy of the control body, J/kg. k_{eff} is the effective heat transfer coefficient, W/(m·k). h_j is the enthalpy of the j component, J/kg. J_j is the diffusion flux of the j component, kg/(m^2·s). S_h is the chemical reaction heat, J.

In the k equation ρ is the fluid density, k is the turbulent kinetic energy, u_j is the velocity component, μ is the kinetic viscosity, σ_k is the correction factor, μ_t is the turbulent kinetic viscosity, P_k is the turbulent energy generation term, and ρ_ε is the turbulence dissipation rate.

In the ω equation, ω is the turbulent dissipation rate, σ_ω is the correction coefficient, P_ω is the turbulent dissipation rate generation term, and C_{lim} is the limiting factor.

Due to the change of pressure and temperature in the injection process of supercritical CO_2, its working parameters will gradually reach the phase equilibrium temperature and absorb heat to become gaseous. This process is accompanied by the transfer of mass and energy, which is the key problem of supercritical CO_2 injection simulation. In this study, the Lee model is used to simulate the mass transfer process between gas and liquid phases of CO_2. The determination conditions for phase change mass transfer are when the temperature of CO_2 is greater than the saturation temperature at the corresponding pressure and the volume fraction of the supercritical phase is greater than 0; the supercritical phase is transferred to the gas phase. The mass transfer source term is expressed as follows:

$$S_m = \beta\alpha_l\rho_l\frac{T - T_{sat}}{T_{sat}} \quad (6)$$

The process of the CO_2 phase change mass transfer corresponds to the transfer of energy. The energy source term can be written as

$$S_T = -h_{lg}\beta\alpha_l\rho_l\frac{(T_l - T_{sat})}{T_{sat}} \quad (7)$$

where T is the vapor pressure, T_{sat} is the saturation pressure, β is the relaxation time, and α_l and ρ_l are the volume fraction and density of the single phase, respectively. In order to accurately describe the leakage and diffusion phenomenon of supercritical CO_2, transient- and pressure-based methods are used to solve the numerical simulation. The mixture model is used for the multiphase flow model; the energy model and the component transport model are in use; the $k-\omega$ SST model is used for the turbulence model; and the coupling problem of pressure and velocity is solved by the coupled algorithm. The volume fraction equation is discretized by QUICK scheme, and the momentum equation, turbulent kinetic energy equation, and component transport equation are discretized by a second-order upwind scheme. Due to the coupling of high-speed flow and rapid phase transition in the leakage process, the dynamic time step of 10^{-7} to 10^{-4} s can accurately capture the subtle changes of concentration and temperature fields without divergence.

2.3. Boundary Conditions. The following boundary conditions were set.

(1) Inlet: The section of the leakage adopts the pressure inlet boundary, the direction is vertical to the boundary, and the corresponding pressure temperature value is given.

(2) Outlet: The six surfaces of the external flow field are all set as pressure outlets, and the direction adopts a vertical boundary. The pressure value is taken as an atmospheric pressure, that is, 101325 Pa, and the temperature is set to 303 K.

(3) Wall: All facilities and buildings are utilized on the offshore platform, using nonslip and adiabatic conditions.

2.4. Model Validation. Before full-scale supercritical CO_2 leakage simulation, it is necessary to verify the accuracy of the numerical models. In order to conduct the model validation, a series of gas phase CO_2 leakage experiments were performed using a model platform built based on similarity theory. To compare with the experimental data, the size of the simulated offshore platform is also reduced to the original 1/16 so that the size is the same as the model platform used in the experiment. In the validation simulation, the leakage pressure is set to 2.6 MPa, the leakage pipe diameter is set to 6.2 mm, and the leakage temperature is set to 303 K. The simulation calculation started from the leakage to 90 s after the leakage. Figure 3 shows the layout diagram of the CO_2 concentration sensors on the platform.

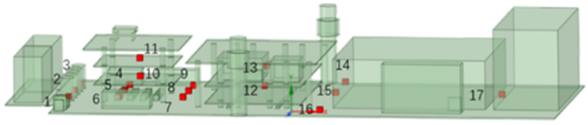

Figure 3. Layout diagram of the CO_2 concentration sensors on the upper platform.

Figure 4 is the temperature field plane simulated at the bottom of the platform. The leakage time is 40 s after the start of leakage. The leakage is steady state during this period. It can be seen from the Figure 4 that although the leakage is a single-phase CO_2 gas, due to the Joule−Thompson effect, there is a certain temperature drop effect. Compared with supercritical conditions, there is no large-area temperature drop, and the temperature drop is small, not more than 1 °C.

Concentration is the key parameter of the model verification. This verification compares several positions with the same position of the experimental concentration sensor. This verification selects leakage monitoring point 5 and leakage

https://doi.org/10.1021/acsomega.4c03002
ACS Omega 2024, 9, 27537−27548

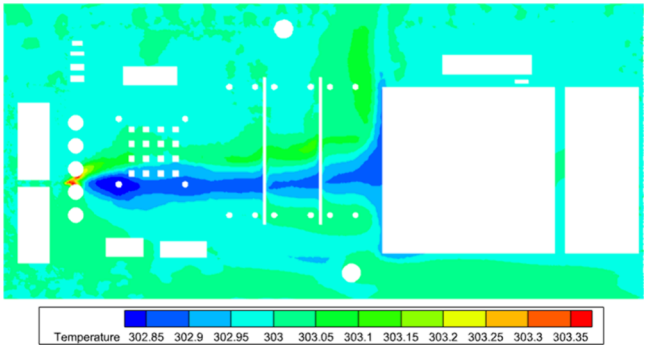

Figure 4. Temperature field of the plane 0.02 m above the bottom of the platform.

monitoring point 8 for comparison. These two points are located on the bottom plane of the offshore platform and are on the same axial plane as the leakage point. The distance between leakage monitoring point 5 and the leakage point is 0.85 m, and the distance between leakage monitoring point 8 and the leakage point is 1.45 m.

The comparison results of the simulation and experiment are shown in Figure 5. It can be seen that in the initial 20 s, the concentration of the experimental sensor is gradually increasing due to the relatively slow response time, and the simulation result reaches a relatively stable value quickly. After 20 s, the increase of the concentration monitored by the sensor in the experiment is greatly reduced, and the concentration reaches a relatively stable state at 40 s. At this time, compared with the simulation results, it is found that the two results are in good agreement at monitoring point 5, and the deviation is smaller than 1%. The simulation results of monitoring point 8 are higher than the experimental results, and the deviation is about 10%. The reason may be that the experiments are conducted in an open environment and monitoring point 8 is far away from the leakage point relative to monitoring point 5, which is affected by the surrounding environment, resulting in simulation results being higher than the experimental results. Because supercritical CO_2 will phase into gaseous CO_2 after throttling after leakage, the use of gas-phase validation reflects the accuracy of the simulation; Figure 6 shows the mass fraction concentration

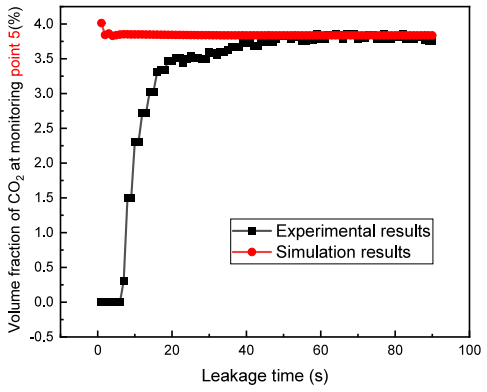

(a) Monitoring point 5

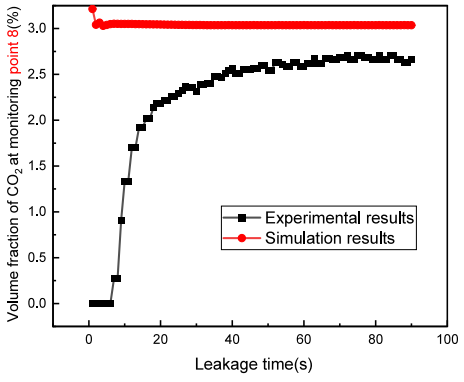

(b) Monitoring point 8

Figure 5. Experimental simulation concentration comparison diagram.

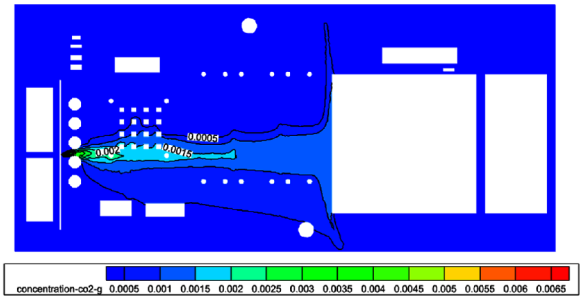

(a) 0.08 m from the bottom of the platform

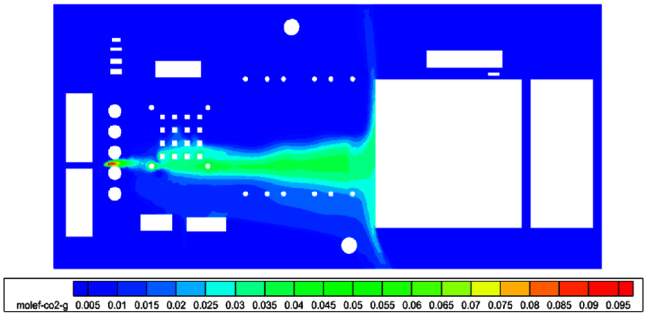

(b) Bottom section of the platform

Figure 6. Gaseous CO_2 volume fraction cloud section.

cloud section of the platform gaseous CO_2 diffusion under steady state. It can be seen that gaseous CO_2 is ejected from the leakage point and then blocked by the offshore platform. The CO_2 concentration is the highest near the leakage point. Under the bottom section of the platform, gaseous CO_2 reaches 9.5% at the leakage point.

3. RESULTS AND DISCUSSION

This section mainly discusses the full-scale simulation of the platform, the change of the temperature, and the CO_2 concentration of the offshore platform with time after the leakage and diffusion of supercritical CO_2. The conditions of the numerical simulation are shown in Table 1.

In order to better analyze the distribution of temperature field and concentration field and identify the dangerous area of offshore platform after CO_2 leakage, the upper offshore platform is divided into front side, rear side, left side, middle side, and right side. The DES and DSM area is the area on the offshore

https://doi.org/10.1021/acsomega.4c03002
ACS Omega 2024, 9, 27537−27548

Table 1. Simulation Conditions

Phase state	Leakage direction	Size of leakage orifice/mm	Leakage time/s	Platform
supercritical	horizontal	100	90	upper
supercritical	horizontal	100	3	middle
supercritical	oblique upward 45°	100	30	upper

platform near the pipeline, the name of which is defined by the CNOOC, and consists of three decks for staff to carry out offshore operations. There are three layers in the DES area of the offshore platform, and the upper cuboid structure is the manhole cover. The DSM region also has three layers, as shown in Figure 7. The structure of the offshore platform affects the direction of

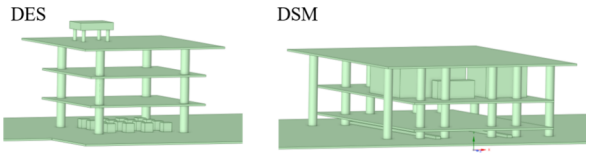

Figure 7. DES and DSM regions of the offshore platform.

carbon dioxide diffusion: 16 manhole covers on the upper level of the DES area trap a large amount of carbon dioxide in them, while the top plate on the upper level hinders the forward diffusion of carbon dioxide; the rear side of the platform is relatively empty, with fewer facilities, and the diffusion of carbon dioxide is less constrained, so that the carbon dioxide diffuses more toward the rear side of the platform. The escape route is between the DES and DMS areas behind the Dsm area of the offshore platforms.

The upper well cover area of DES and the escape channel at the edge of the offshore platform are the main active areas of workers. If the concentration of CO_2 in these areas is too high or the ambient temperature is too low, it will affect the safety of workers. The middle leakage orifice is at leakage point 4, as shown in Figure 8.

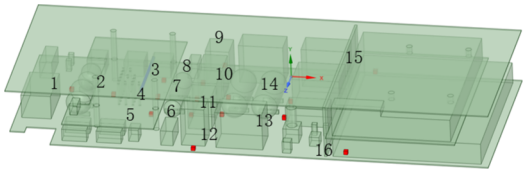

Figure 8. Middle-level offshore platform model.

3.1. Horizontal Leakage on the Upper Platform. After the leakage of supercritical CO_2, it expands to the environmental pressure in the form of an expanded jet. During the expansion process, the jet is significantly cooled due to the Joule−Thomson effect, and phase transition occurs at the same time. The change of phase state will also absorb environmental heat and reduce the temperature. In the following, three planes are selected to analyze the change of temperature with time after supercritical CO_2 leakage and analyze the change of concentration temperature at two heights of 0.5 and 1.7 m from the platform. Subsequently, the three-dimensional cloud diagram of the concentration and the contour map of the temperature at 240 K and the contour map of the concentrations at 1, 5, and 10% were given, and the change process of the temperature concentration was analyzed.

Figure 9 shows the temperature field analysis at different times and different heights. It can be seen that, with the passage of

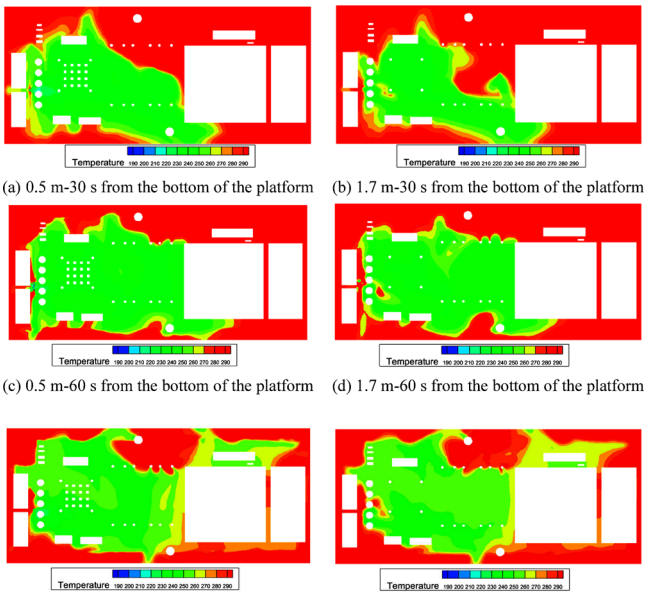

(a) 0.5 m-30 s from the bottom of the platform (b) 1.7 m-30 s from the bottom of the platform

(c) 0.5 m-60 s from the bottom of the platform (d) 1.7 m-60 s from the bottom of the platform

(e) 0.5 m-90 s from the bottom of the platform (f) 1.7 m-90 s from the bottom of the platform

Figure 9. Temperature field changes at different heights and different times.

time, the influence range of low temperature is gradually expanding and the gradient of temperature change is very fast. There is a gap of 30 °C within 1 m, which spreads from the left side of the offshore platform to the middle side at the beginning. Moreover, at 90 s, it has spread to the right side of the platform, and the overall temperature has rebounded.

Figure 10 is the leakage axial plane temperature schematic diagram; as can be seen, at 30 s, only the upper and middle layers

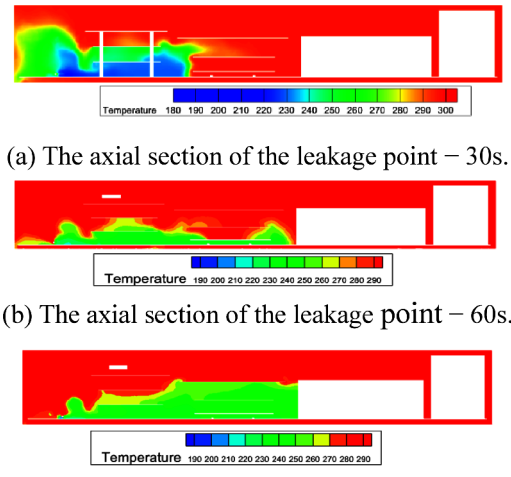

(a) The axial section of the leakage point − 30s.

(b) The axial section of the leakage point − 60s.

(c) The axial section of the leakage point – 90s.

Figure 10. Axial plane temperature change of the leakage point.

of the offshore platform DES are affected. At 60 s, the upper layer temperature reaches about 240 K and spreads to the middle layer. The temperature of the middle layer drops to 270 K, the temperature rises at 90 s, and the temperatures of the upper and middle layers of the DES reach about 240 K.

https://doi.org/10.1021/acsomega.4c03002
ACS Omega 2024, 9, 27537−27548

Figure 11 is the temperature contour map of 240 K at different times. It can be seen that at 30 s, the 240 K contour surface

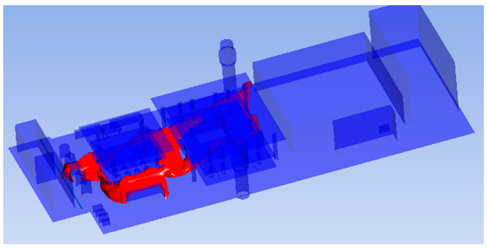

(a) Leakage time 30s

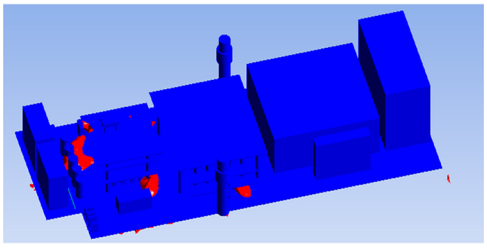

(b) Leakage time 60s

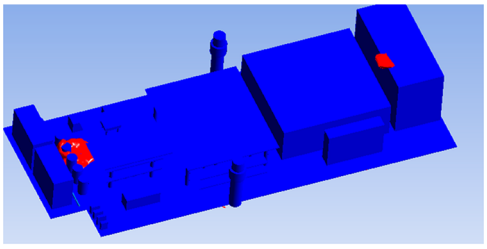

(c) Leakage time 90s

Figure 11. Isosurface at 240 K.

spreads to the middle of the offshore platform and gathers in the upper layer of DES. At 60 s, the range of the 240 K contour surface is reduced, which is due to the lower temperature drop of the platform. The 240 K contour surface is reduced near the leakage point. At 90 s, the area of the temperature contour surface is smaller, which is also due to the lower temperature drop on the platform.

Figure 12 shows the temperature changes of different points on the offshore platform over time. The positions of the selected points on the offshore platform are shown in Figure 13. It can be seen that there is a significant drop in temperature once the leakage starts at the monitoring point near the leakage point and the temperature remains consistent with the simulation time. The temperature in the middle of the offshore platform drops to about −40 °C at 30 s. The rightmost point of the offshore platform begins to drop in temperature at 70 s.

Figure 14 shows the variation of the concentration field at different heights and times. When the leakage time is 30 s, CO_2 is mainly concentrated on the left and middle sides of the offshore platform and a small amount of CO_2 diffuses to the escape channel. The concentration of CO_2 in the upper layer and tank area of the DES area is up to 70%, and the CO_2 concentration range on the escape channel is 50−70%.

When the leakage time is 60 s, the CO_2 concentration on the left side of the offshore platform decreases, the CO_2

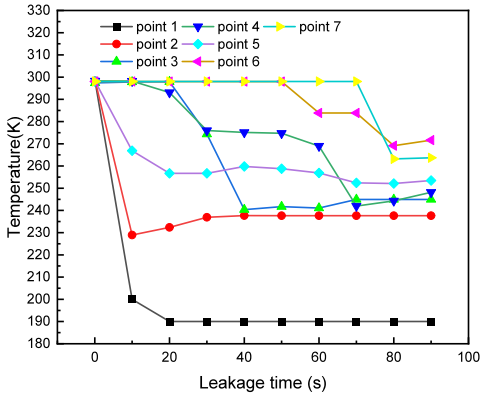

Figure 12. Temperature changes with time at different positions of the offshore platform.

concentration in some areas of DES decreases from 70 to 50% or lower, and the concentration in other areas decreases more. When the leakage time is 60 s, CO_2 begins to diffuse to the rear side of the offshore platform, and the concentration of the middle and rear escape channels reaches 40%.

When the leakage time is 90 s, the maximum concentration of CO_2 in the upper layer of the DES area is 50%, and the overall CO_2 concentration of the platform seems to decrease. This may be due to the effect of gravity, in which more CO_2 is deposited to the bottom of the platform.

Figure 15 shows the 3D concentration changes. It can be seen that as time goes on the concentration of CO_2 gradually spreads to the middle of the offshore platform. Blocked by the right building, CO_2 is gathered here in large quantities and the aggregation height increases.

Figure 16 shows the isosurface diagram of CO_2 with concentrations of 1, 5, and 10%. It can be seen from the figure that the range of the level of CO_2 is quite close among these three values. At 30 s, most of the CO_2 is still concentrated in the middle of the offshore platform. At 60 s, CO_2 has basically spread to all parts of the offshore platform. At 90 s, 10% has spread to the right side of the offshore platform.

Figure 17 shows the change of concentration with time at different positions of the offshore platform. It can be seen that the concentration near the leakage point is stable at 90% once leakage occurs, while the concentration of the monitoring point on the right side of the offshore platform begins to increase at 70 s.

According to the above discussions, it can be analyzed that, with the increase of leakage time, the change of the CO_2 concentration cloud map shows the following rules:

(1) The concentration of CO_2 on the left side of the platform decreases gradually: the concentration of CO_2 in the tank area and DES area decreases mainly because of the increase of CO_2 leakage, the large downward settlement of CO_2 affected by gravity, and the regional structure limits the diffusion of CO_2. On the one hand, the concentration of the left open area decreases due to the gravity of CO_2, and on the other hand, it diffuses backward.

(2) The offshore platform structure affects the diffusion direction of CO_2: there are 16 manhole covers in the upper layer of the DES area to trap a large amount of CO_2, and the upper roof hinders the forward diffusion of CO_2. The rear side of the platform is relatively open, with fewer facilities, and the diffusion of CO_2 is less restricted, so CO_2 diffuses more to the rear side of the platform.

https://doi.org/10.1021/acsomega.4c03002
ACS Omega 2024, 9, 27537−27548

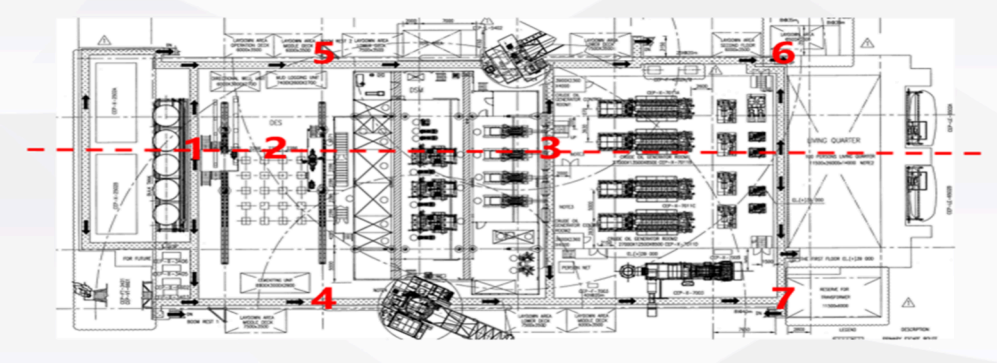

Figure 13. Location of different monitoring points on an offshore platform.

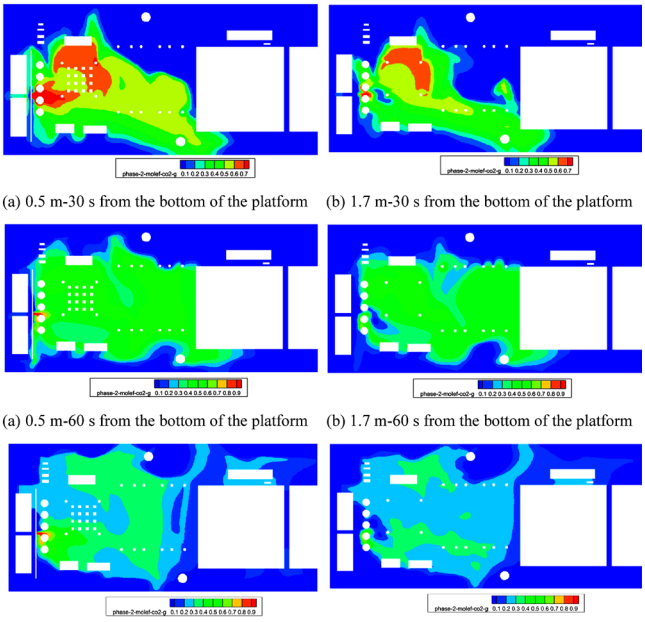

(a) 0.5 m-30 s from the bottom of the platform (b) 1.7 m-30 s from the bottom of the platform

(a) 0.5 m-60 s from the bottom of the platform (b) 1.7 m-60 s from the bottom of the platform

(a) 0.5 m-90 s from the bottom of the platform (b) 1.7 m-90 s from the bottom of the platform

Figure 14. Variation of the concentration field at different heights and different times.

(3) The influence area of CO_2 in the rear escape channel increases, and the concentration is maintained at 20%. The diffusion of CO_2 in the rear escape channel of the platform is not hindered, and the influence area increases with time. The diffusion of CO_2 on the middle and rear sides of the offshore platform is mainly passive diffusion. Far away from the leakage source, CO_2 is diluted by air, and gravity and buoyancy tend to balance. Therefore, the concentration of CO_2 at 1.7 m above the escape channel on the rear side of the platform is relatively stable.

The Emergency & Critical Care Pocket Guide points out that when the indoor CO_2 concentration reaches 5%, it will cause early symptoms such as headache, fatigue, dyspnea, and nausea. When the concentration reaches 8%, sharp reactions, such as increased heart rate, elevated blood pressure, difficulty in concentration, and blurred vision, begin to appear, which is very dangerous. Finally, when the concentration reaches 10%, people quickly lose consciousness and may die within a few minutes. According to the figures above, as the leakage time increases, the area where the CO_2 concentration exceeds 10% on plane m gradually increases. When the leakage time is 30 s, the concentrations in the tank area and DES area are as high as

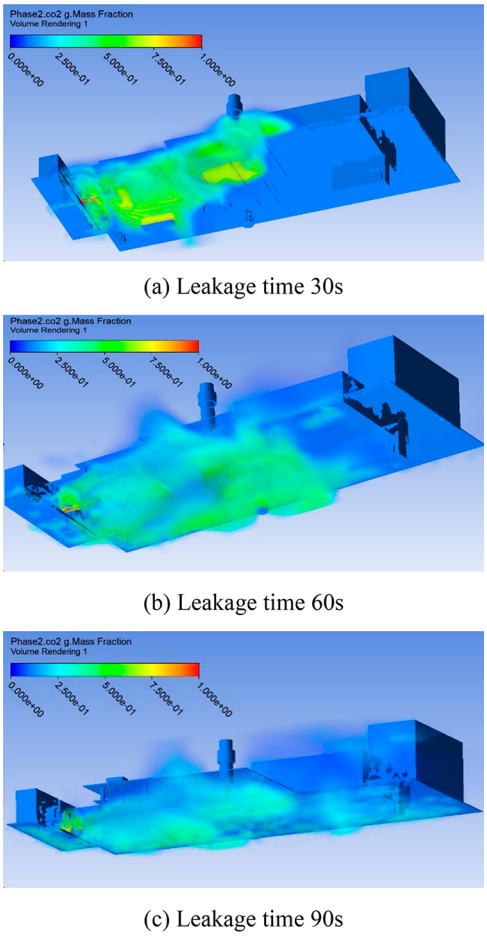

(a) Leakage time 30s

(b) Leakage time 60s

(c) Leakage time 90s

Figure 15. Three-dimensional variation of concentration.

70%. It should be pointed out that more than 30% of the CO_2 concentration has far exceeded the risk values listed in the above report, which is an extremely abnormal situation and will seriously endanger people's life and health. The DES area and the rear escape channel of the platform are personnel-intensive areas. If supercritical CO_2 leakage occurs, it will seriously endanger the lives and health of workers in a very short time. It is crucial to take measures to prevent supercritical CO_2 leakage and develop plans for escape after supercritical CO_2 leakage. This article suggests that, in the event of a supercritical CO_2 leakage, workers in the DES area should quickly evacuate from the front escape channel of the offshore platform, while workers in the rear escape channel of the offshore platform can quickly

https://doi.org/10.1021/acsomega.4c03002
ACS Omega 2024, 9, 27537−27548

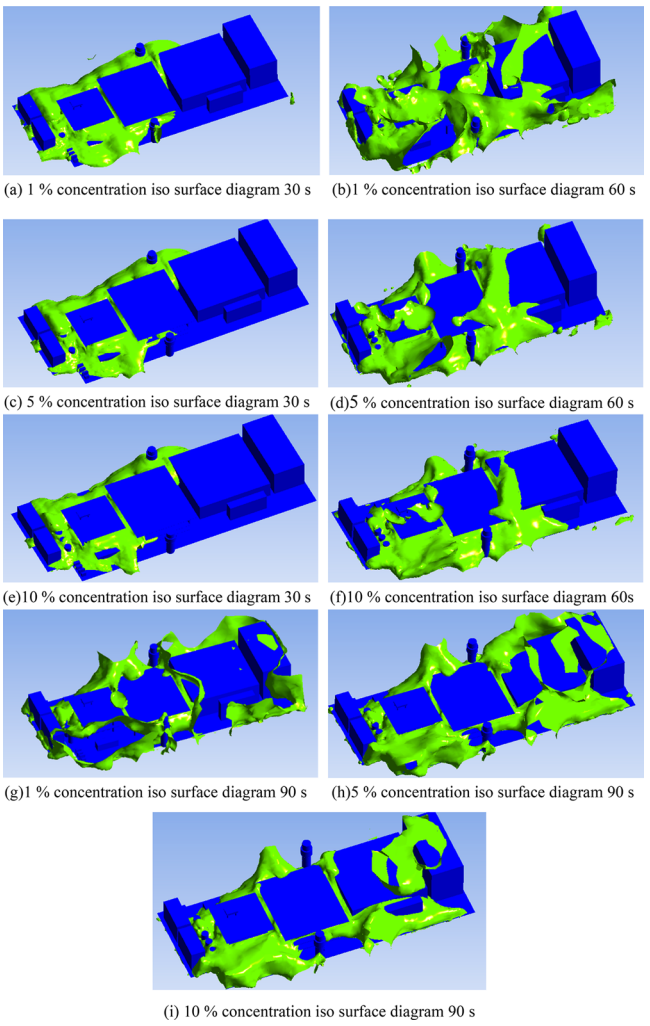

Figure 16. Isosurfaces of different concentrations of offshore platforms.

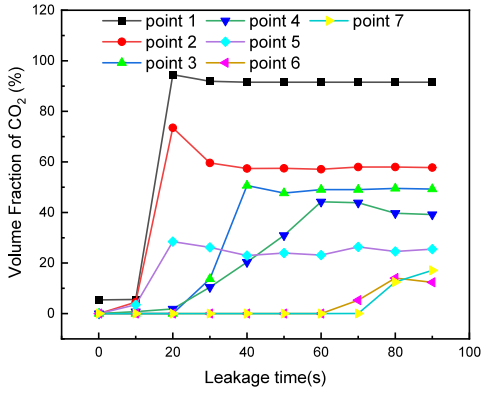

Figure 17. Changes of the concentration of monitoring points on the offshore platform.

flee toward the left or right edge of the platform; When staff members escape, they should avoid going to open areas and utilize equipment, facilities, and large buildings to hinder the diffusion of CO_2.

3.2. Horizontal Leakage on the Middle Platform. Due to the complex structure of the middle layer, frequent errors are reported in the calculation. After numerous simplifications and corrections to the geometric model, it is possible to run, and because the structure is more complex than the upper layer, the calculation is very slow. At present, the results after 3 s of leakage are given. In the following, the changes of concentration and temperature are analyzed at two heights of 0.5 and 1.7 m from the platform.

Figure 18 shows the cross-section cloud diagram of the CO_2 temperature at different heights. It can be seen from Figure 18

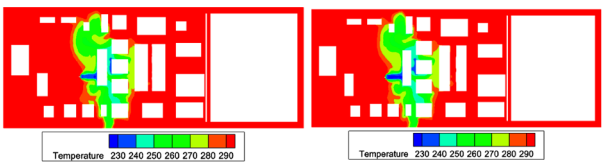

(a) 0.5 m from the bottom of the platform (b) 1.7 m-3 s from the bottom of the platform

Figure 18. Cross-section of the CO_2 temperature at different heights.

that the temperature of the leakage point drops to 230 K 3 s after leakage.

Figure 19 shows the cross-section cloud diagram of the CO_2 concentration at different heights. It can be seen from Figure 19

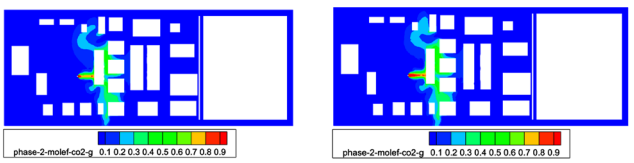

(a) 0.5 m from the bottom of the platform (b) 1.7m-3s from the bottom of the platform

Figure 19. Isosurfaces of the CO_2 concentration at different heights.

that the concentration on both sides of the platform reaches 0.2 at 3 s after leakage.

Figure 20 is a 3D concentration change map of CO_2. It can be seen that as time goes on, the concentration of CO_2 gradually

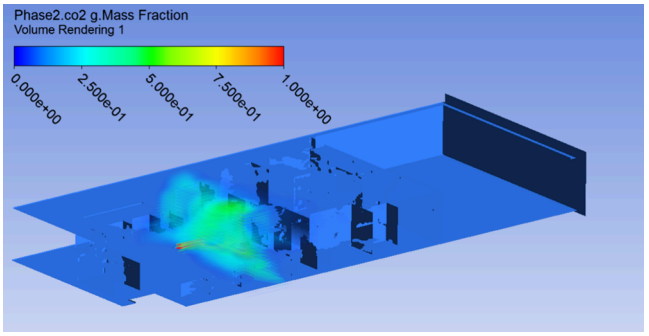

Figure 20. 3D CO_2 concentration map.

spreads to the middle of the offshore platform, which is blocked by the right building. CO_2 is gathered here in large quantities due to the increase of aggregation height.

3.3. Oblique Upward 45° Leakage on the Upper Platform. The leakage point of this working condition is inclined to 45° upward, and other conditions are the same as those of the first working condition.

Figure 21 shows the temperature field analysis at different heights and different times. At 30 s, the low-temperature area is mainly concentrated on the left and middle sides of the platform. As the leakage time increases, a small amount of CO_2 diffuses to the right side of the offshore platform, causing a temperature drop in some areas.

https://doi.org/10.1021/acsomega.4c03002
ACS Omega 2024, 9, 27537−27548

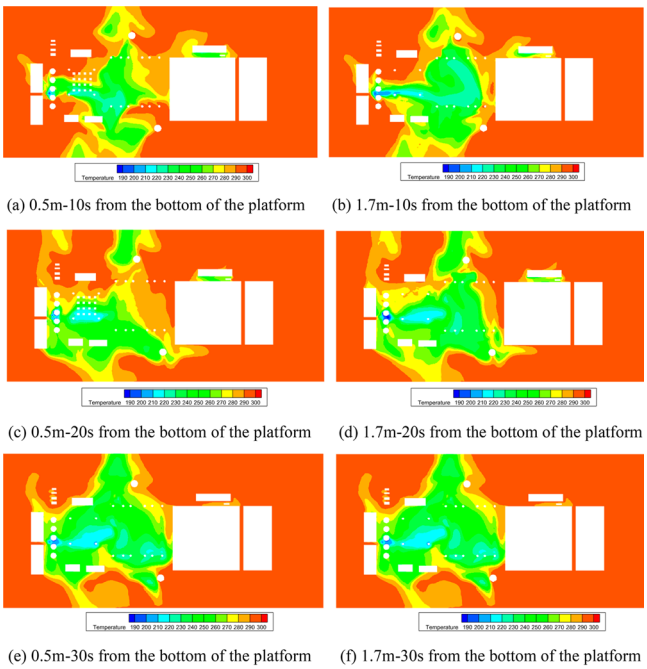

Figure 21. Temperature field changes at different heights and different times.

Figure 22 shows the cloud diagram of the axial plane temperature of the leakage point changing with time, and the

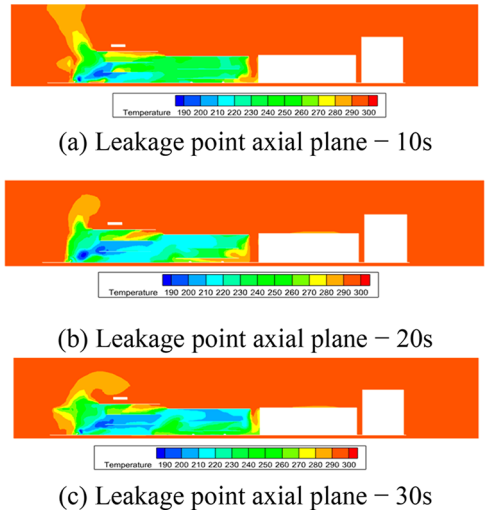

Figure 22. Axial plane temperature of the leakage point changes with time.

leakage times are 10, 20, and 30 s, respectively. When the leakage time is 10 s, the lowest temperature of the leakage point along the wind and the tank area is 220 K, which is due to the low temperature caused by expansion of the near-field jet after the CO_2 leakage. Due to the leakage angle, the area where the temperature is lower than 250 K is mainly concentrated in the tank area and the channel of all three layers of DES.

When the leakage time is 20 s, the temperature of the upper part of the DSM area is reduced to 230 K. This is because the leakage time increases, the leakage amount increases, and the CO_2 is more affected by gravity than buoyancy and the temperature increases.

When the leakage time is 30 s, the CO_2 is diffused, the area of the tank area near the leakage point with a temperature of 220 K is reduced, and the temperature of the upper layer of the DES area and the upper layer of the DSM is 200 K, which is reduced. The overall temperature drop area is greatly reduced, which is due to the entrainment effect of CO_2 and air.

Figure 23 shows the isosurface diagram of 240 K at different times (30 s). The 240 K isosurface spreads to the middle side of the offshore platform and changes little within 30 s.

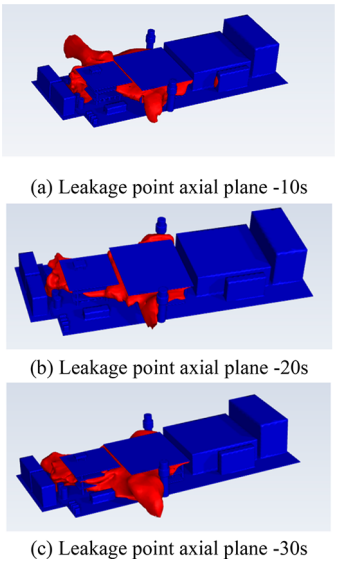

Figure 23. Isosurface of 240 K.

Figure 24 shows the temperature changes of different points on the offshore platform with time. Similarly, monitoring point 1

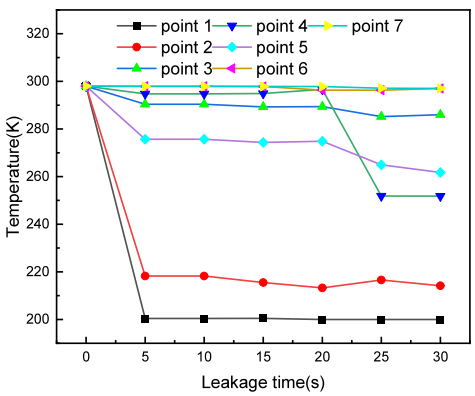

Figure 24. Temperature of different points on the offshore platform changes with time.

near the leakage point has a significant temperature drop as soon as it starts to leak, and the temperature remains the same as the simulation time. Monitoring points 4 and 5 begin to drop at about 20 s, while the right side of the offshore platform (monitoring points 6 and 7) does not drop in 30 s.

Figure 25 shows the change of the concentration field with time. With the increase of leakage time, the concentration of CO_2 in the DES area decreases due to the influence of gravity. After the CO_2 in the rear escape channel is diluted by air, the gravity and buoyancy balance and the concentration remain unchanged. Affected by the structure of the offshore platform,

https://doi.org/10.1021/acsomega.4c03002
ACS Omega 2024, 9, 27537−27548

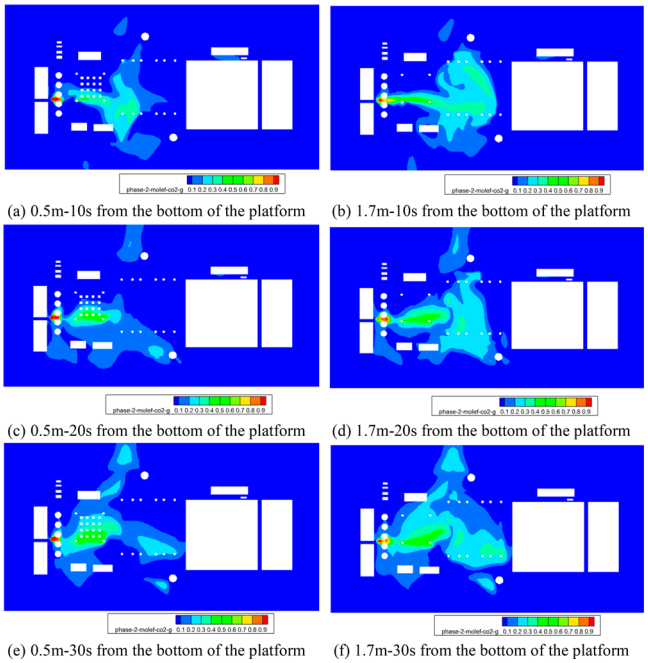

Figure 25. Variation of the concentration field at different heights and different times.

some CO_2 will accumulate in the upper layer of the DES area, and the diffusion direction of CO_2 mainly tends to the rear side of the platform; therefore, the DES area and the rear escape channel of the platform are extremely dangerous areas.

Figure 26 shows the concentration cloud diagram of gaseous CO_2 diffusion at different times. It can be seen that a 1% concentration has spread to all offshore platforms at 10 s. Compared with horizontal leakage, it shows that 45° oblique upward leakage is more dangerous. CO_2 is affected by gravity and air entrainment and will spread farther.

Figure 27 shows the concentration changes of different points on the offshore platform over time. Once monitoring point 1 near the leakage point reaches 95%, and the concentration remains the same as the simulation time, the concentrations of monitoring points 4 and 5 begin to increase at about 20 s, while the right side of the offshore platform (monitoring points 6 and 7) does not change in concentration within 30 s. Different from the horizontal leakage, the point concentration on the 45° leakage platform fluctuates after the leakage.

4. CONCLUSIONS

In this work, a series of numerical simulations are conducted to study the temperature and concentration distributions on an offshore platform after pipeline supercritical CO_2 leakage and diffusion happened. The main conclusions of this work are listed as follows.

(1) When the horizontal leakage occurs, the upper and middle layers of DES will be greatly affected, and the temperature will drop to about −40 °C. When the leakage point is inclined upward, all of the three DES layers are greatly affected. In summary, in the event of leakage, the staff in the DES area should be evacuated as soon as possible and the pipeline material must have high strength and high toughness to prevent the spread of cracks.

(2) With the increase of leakage time, CO_2 in the DES region is affected by gravity to sink downward, resulting in a decrease in concentration. After CO_2 in the rear escape channel is diluted by air, the gravity and buoyancy balance and the concentration remain unchanged. Affected by the structure of the offshore

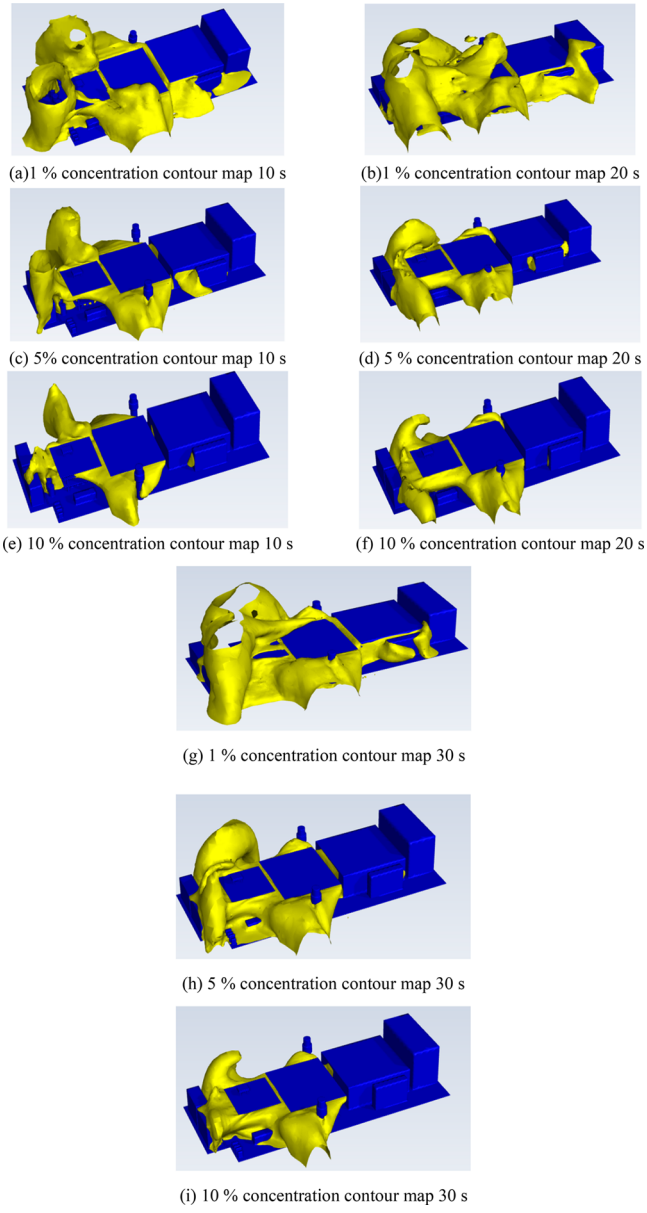

Figure 26. Concentration contour map.

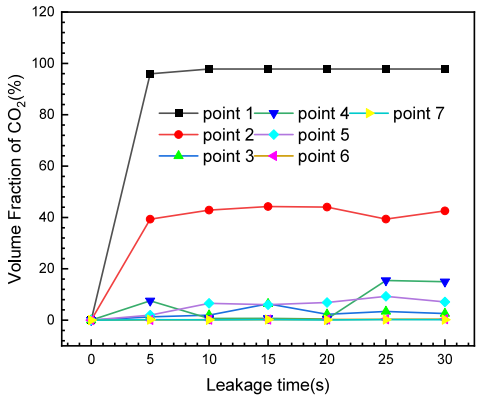

Figure 27. Concentration of different points on the offshore platform changes with time.

https://doi.org/10.1021/acsomega.4c03002
ACS Omega 2024, 9, 27537−27548

platform, part of the CO_2 will accumulate in the upper layer of the DES region, and the CO_2 mainly tends to diffuse to the back side of the platform, so the DES region and the escape channel at the back side of the platform are extremely dangerous areas.

(3) After the leakage of supercritical CO_2, the upper and rear escape channels of DES in densely populated areas will be harmed by the low-temperature and high-concentration CO_2. It is recommended to evacuate the DES area personnel through the escape channel in front of the platform, and the staff in the back escape channel are advised to evacuate to the left and right edges of the platform. When evacuating, staff need to make reasonable use of the hindrance effect of offshore platform equipment and facilities and buildings on CO_2 diffusion to gain time for evacuation.

(4) When supercritical CO_2 leaks, the influence of low temperature is significantly larger than that of gaseous CO_2 leaks, and the temperature drops to about −80 °C; the upper and middle layers of DES receive a relatively large impact when leaking horizontally and the temperature drops to −40 °C, and all three layers of the DES platform receive a relatively large impact when the leakage port leaks obliquely upward. In summary, once a leak occurs, staff in the DES area should be evacuated as soon as possible and the piping material must have the ability to prevent crack propagation with high strength and toughness. Regarding the analysis of the CO_2 concentration field, the safe evacuation of the DES platform should be ensured no matter what the direction of leakage is.

AUTHOR INFORMATION

Corresponding Author

Guangchun Song − *College of Pipeline and Civil Engineering, China University of Petroleum, Qingdao 266580 Shandong, China;* orcid.org/0000-0001-8485-772X; Email: UpcNGH_sgc@163.com

Authors

Yang Cao − *CNOOC Research Institute Ltd., Beijing 100028, China; CNOOC China Ltd., Beijing Research Center, Beijing 100028, China*

Tao Liu − *CNOOC Research Institute Ltd., Beijing 100028, China; CNOOC China Ltd., Beijing Research Center, Beijing 100028, China*

Wei Zhou − *CNOOC Research Institute Ltd., Beijing 100028, China; CNOOC China Ltd., Beijing Research Center, Beijing 100028, China*

Hui Han − *College of Pipeline and Civil Engineering, China University of Petroleum, Qingdao 266580 Shandong, China*

Yuxing Li − *College of Pipeline and Civil Engineering, China University of Petroleum, Qingdao 266580 Shandong, China*

Qihui Hu − *College of Pipeline and Civil Engineering, China University of Petroleum, Qingdao 266580 Shandong, China*

Ruidong Jing − *College of Pipeline and Civil Engineering, China University of Petroleum, Qingdao 266580 Shandong, China*

Complete contact information is available at: https://pubs.acs.org/10.1021/acsomega.4c03002

Notes

The authors declare no competing financial interest.

ACKNOWLEDGMENTS

This work was supported by China National Offshore Oil Corp. (CNOOC), National Natural Science Foundation of China (No. 52104070), National Key Research and Development Program of China (No. 2022YFE0206800), and Natural Science Foundation of Shandong Province, China (ZR2021QE169, ZR2022QE038), which are gratefully acknowledged.

REFERENCES

(1) Al Baroudi, H.; Awoyomi, A.; Patchigolla, K.; Jonnalagadda, K.; Anthony, E.J. A review of large-scale CO_2 shipping and marine emissions management for carbon capture, utilisation and storage. *Appl. Energy* **2021**, *287*, 116510.

(2) Lu, H. F.; Ma, X.; Huang, K.; et al. Carbon dioxide transport via pipelines: A systematic review[J]. *J. Cleaner Prod.* **2020**, *266*, 121994.

(3) Onyebuchi, V. E.; Kolios, A.; Hanak, D. P.; et al. A systematic review of key challenges of CO_2 transport via pipelines[J]. *Renewable Sustainable Energy Rev.* **2018**, *81*, 2563−2583.

(4) Ding, H. B.; Zhang, Y.; Dong, Y. Y.; et al. High-pressure supersonic carbon dioxide (CO2) separation benefiting carbon capture, utilization and storage (CCUS) technology[J]. *Appl. Energy* **2023**, *339*, 120975.

(5) Smith, E.; Morris, J.; Kheshgi, H.; et al. The cost of CO_2 transport and storage in global integrated assessment modeling[J]. *Int. J. Greenhouse Gas Control* **2021**, *109*, 103367.

(6) Hill, L. B.; Li, X. C.; Wei, N. CO_2-EOR in China: A comparative review[J]. *Int. J. Greenhouse Gas Control* **2020**, *103*, 103173.

(7) Bachu, S. CO_2 storage in geological media: Role, means, status and barriers to deployment[J]. *Prog. Energy Combust. Sci.* **2008**, *34* (2), 254−273.

(8) Farajzadeh, R.; Eftekhari, A. A.; Dafnomilis, G.; et al. On the sustainability of CO_2 storage through CO_2 - Enhanced oil recovery[J]. *Appl. Energy* **2020**, *261*, 114467.

(9) Roberts, J. J.; Stalker, L. What have we learnt about CO_2 leakage from CO_2 release field experiments, and what are the gaps for the future?[J]. *Earth-Sci. Rev.* **2020**, *209*, 102939.

(10) Li, K.; Zhou, X. J.; Tu, R.; et al. The flow and heat transfer characteristics of supercritical CO_2 leakage from a pipeline[J]. *Energy* **2014**, *71*, 665−672.

(11) Gu, S. W.; Li, Y. X.; Teng, L.; et al. The flow and heat transfer characteristics of supercritical CO_2 leakage from a pipeline[J]. *Process Safe. Environ. Protect.* **2019**, *125*, 92−101.

(12) Zhou, X. J.; Li, K.; Tu, R.; et al. A modelling study of the multiphase leakage flow from pressurized CO_2 pipeline[J]. *J. Hazard. Mater.* **2016**, *306*, 286−294.

(13) Gale, J.; Davison, J. Transmission of CO_2—safety and economic considerations[J]. *Energy* **2004**, *29* (9−10), 1319−1328.

(14) Hu, Y. W.; Yan, X. Q.; Chen, L.; et al. Leakage hazard distance of supercritical CO_2 pipelines through experimental and numerical studies[J]. *Int. J. Greenhouse Gas Control* **2022**, *119*, 103730.

(15) Vitali, M.; Zuliani, C.; Corvaro, F.; et al. Risks and safety of CO_2 transport via pipeline: A review of risk analysis and modeling approaches for accidental releases[J]. *Energies* **2021**, *14* (15), 4601.

(16) Teng, L. The leakage and dispersion characteristics and quantitative risk assessment of supercritical CO_2 released from pipelines. Ph.D. Thesis, China University of Petroleum, Qing Dao, East China, 2019.

(17) Jensen, M. D.; Pei, P.; Snyder, A. C.; et al. Methodology for phased development of a hypothetical pipeline network for CO_2 transport during carbon capture, utilization, and storage[J]. *Energy Fuels* **2013**, *27*, 4175−4182.

(18) Wang, C. L.; Li, Y. X.; Teng, L.; et al. Experimental study on dispersion behavior during the leakage of high pressure CO_2 pipelines[J]. *Exp. Therm. Fluid Sci.* **2019**, *105*, 77−84.

(19) Teng, L.; Li, Y. X.; Hu, Q. H.; et al. Experimental study of near-field structure and thermo-hydraulics of supercritical CO_2 releases[J]. *Energy* **2018**, *157*, 806−814.

(20) Teng, L.; Li, Y. X.; Zhang, D. T.; et al. Evolution and size distribution of solid CO_2 particles in supercritical CO_2 releases[J]. *Ind. Eng. Chem. Res.* **2018**, *57*, 7655−7663.

(21) Guo, X. L.; Yan, X. Q.; Yu, J. L.; et al. Under-expanded jets and dispersion in supercritical CO_2 releases from a large-scale pipeline[J]. *Appl. Energy* **2016**, *183*, 1279−1291.
(22) Guo, X. L.; Chen, S. Y.; Yan, X. Q.; et al. Flow characteristics and dispersion during the leakage of high pressure CO_2 from an industrial scale pipeline[J]. *Int. J. Greenhouse Gas Control* **2018**, *73*, 70−78.
(23) Ahmad, M.; Lowesmith, B.; Koeijer, G. D.; et al. COSHER joint industry project: Large scale pipeline rupture tests to study CO_2 release and dispersion[J]. *Int. J. Greenhouse Gas Control* **2015**, *37*, 340−353.
(24) Witlox, H. W. M.; Harper, M.; Oke, A.; et al. Phast validation of discharge and atmospheric dispersion for pressurized carbon dioxide releases[J]. *J. Loss Prevent. Process Ind.* **2014**, *30*, 243−255.
(25) Witlox, H. W. M.; Harper, M.; Oke, A.; et al. Validation of discharge and atmospheric dispersion for unpressurised and pressurized carbon dioxide releases[J]. *Process Safe. Environm. Protect,* **2014**, *92* (1), 3−16.
(26) Ahmad, M.; Osch, M. B.; Buit, L.; et al. Study of the thermohydraulics of CO_2 discharge from a high pressure reservoir[J]. *Int. J. Greenhouse Gas Control* **2013**, *19*, 63−73.
(27) Xie, Q. Y.; Tu, R.; Jiang, X.; et al. The leakage behavior of supercritical CO_2 flow in an experimental pipeline system[J]. *Appl. Energy* **2014**, *130*, 574−580.

https://doi.org/10.1021/acsomega.4c03002
ACS Omega 2024, 9, 27537−27548